
Abundance Ratio of Secondary to Primary Expected from the Boundaryless Galaxy Model

Makoto Hareyama, M. Nakazawa, C. Saito, R. Suzuki, and T. Shibata
Department of Physics, Aoyama-Gakuin University, Sagamihara, Kanagawa 229-8558, Japan

Abstract

Based on the boundaryless Galaxy model, we present secondary to primary ratio in the high energy region, $\gtrsim 5 \text{ GeV/n}$, where the low energy effect such as reacceleration and the ionization energy loss is negligible. We focus on two data, B/C and sub-Fe(21-23)/iron, and find reasonable parameters reproducing nicely both data.

We discuss also the anisotropy problem in connection with the parameters we estimate here, gas density n , the diffusion coefficient D and so on.

1. Introduction

In paper I[1], we present a new approach to the cosmic ray propagation, assuming a rather realistic structure of our Galaxy, and find it reproduces well the primary components, proton \sim iron. It is, however, not enough to estimate uniquely many parameters appearing in our model with use of the primary component alone.

In the present paper, we show the solution of the cosmic ray density for the stable secondary components, and compare it with the data on the ratio of secondary to primary nowadays available. Unstable secondary components such as ^{10}Be is presented separately in this proceeding[2].

2. Abundance Ratio of the Secondary to Primary Component

The number density of the secondary component originated from the primary component $N_p(\mathbf{r})$ are straightforwardly given by

$$N_{p \rightarrow s}(\mathbf{r}) = \iint d\mathbf{r}_0 [N_p(\mathbf{r}_0) n(\mathbf{r}_0) v \sigma_{p \rightarrow s}] \Phi_s(\mathbf{r}; \mathbf{r}_0), \quad (1)$$

where we omit the rigidity term R for the sake of simplicity. Here, $\sigma_{p \rightarrow s}$ denotes the fragmentation cross section, p (primary) \rightarrow s (secondary). In the present work we omit the contribution from the second step product (second generation fragments), $p \rightarrow s' \rightarrow s$, since $\sigma_{p \rightarrow s' \rightarrow s}$ is usually much smaller than $\sigma_{p \rightarrow s}$.

The Green function Φ_s is completely the same as Φ_p after replacing the cross section σ_p by σ_s , the cross section of the secondary component with the interstellar gas. Both functions, N_p and Φ_p , are already presented in Paper I, and so we give only the result, detail of which will be reported elsewhere,

$$\frac{N_{p \rightarrow s}(r; R)}{N_p(r; R)} = 4\nu^2 R^{-\alpha} \frac{\sigma_{p \rightarrow s}}{\sigma_r} \frac{\mathcal{I}_{\nu, \nu}(U_{r,R}; \hat{U}_{r,R})}{\hat{U}_{r,R} I_{\nu-1}(\hat{U}_{r,R})}, \quad (2)$$

where all variables, α , ν , and σ_r are the same as those appearing in Paper I. $N_p(r; R)$ and $U_{r,R}$ are defined by Eqs. (7) and (8) in Paper I, and

$$\hat{U}_{r,R} = 2\nu R^{-\alpha/2} \sqrt{\sigma_s/\sigma_r} = U_{r,R} \sqrt{\sigma_s/\sigma_p}, \quad (3)$$

$$\mathcal{I}_{\nu, \eta}(a; \hat{a}) \simeq \int_0^1 t [1 + \nu(1-t) + \dots] I_\eta(\hat{a}t) dt, \quad (4)$$

where the contribution of a appears in the third term in the expansion, which is of the magnitude of less than 10%.

In the limit of $R \rightarrow \infty$ in Eq. (2), we obtain a simple form as expected,

$$\frac{N_{p \rightarrow s}(r; R)}{N_p(r; R)} = \bar{\omega}^2 R^{-\alpha} \frac{\sigma_{p \rightarrow s}}{\sigma_r}, \quad (5)$$

where $\bar{\omega}$ is defined by Eq. (12) in Paper I, related to three scale heights, z_D , z_n and z_Q .

While the present paper is focussed on the high energy region only, $\gtrsim 5$ GeV/n, let us show the secondary to primary ratio in the lower energy limit taking the reacceleration process into account, in order to see the difference from the above result for $R \rightarrow \infty$. The derivation is a little bit cumbersome, but the final result becomes a quite simple and reasonable,

$$\frac{N_{p \rightarrow s}(r; R)}{N_p(r; R)} \approx \frac{4}{3} \frac{\sigma_{p \rightarrow s}}{\zeta_0} \frac{R^\alpha}{\bar{\beta} + 2}, \quad \text{with } \bar{\beta} = \gamma - \alpha, \quad (6)$$

where γ is the exponent of the rigidity spectrum of the primary component at the source, and ζ_0 is the reacceleration efficiency with 100-500mb, the detail of which will be reported elsewhere near future. The most important point we would like to stress here is the rigidity dependence, R^α ($\propto E^{\alpha/2}$), in the lower energy limit, which should be compared with $R^{-\alpha}$ ($\propto E^{-\alpha}$) in the high energy limit, namely we can expect a convex shape in the secondary to primary ratio without introducing an artificial break in the path length somewhere around a few GV, currently assumed in the standard leaky box model.

While this fact has been suggested by many authors[3, 4], our consideration shows more quantitatively in connection with the reacceleration efficiency, ζ_0 , and the exponent of the source, γ , as well as the exponent of the rigidity dependence in the diffusion coefficient, α . More detail consideration including the ionization loss effect will be reported elsewhere.

3. Comparison with the Experimental Data

As presented in Paper I, we find two possible choices in $(\gamma, \alpha) = (2.4 \sim 2.5, 1/3)$, and $(2.2 \sim 2.3, 1/2)$, reproducing the experimental data on the primary spectrum, as long as $\beta (= \gamma + \alpha)$ is fixed to 2.7-2.8. On the other hand, in the case of the ratio of the secondary to primary, γ is cancelled out each other (for high energy region) as seen from Eq. (2). So, in this section we compare the data of the secondary to primary ratio with our model for two choices, a) $\alpha=1/3$ and b) $\alpha=1/2$. The cross section data is based on those compiled by Webber et al.[5].

In Figs. 1a), b), and 2a), b), we show B/C-ratio and sub-Fe/iron-ratio[3, 4, 6], respectively, where two curver-fittings correspond to a): $\alpha=1/3$ with $\sigma_r=2\sigma_0$, and b): $\alpha=1/2$ with $\sigma_r=\sigma_0(=34.94\text{mb}$; see Paper I), for each figure 1 and 2. Both choices reproduce the experimental data well within the fluctuation. We assume $z_Q/z_n=0.5$, $r_n=r_Q=15\text{Kpc}$, though preliminary, which are not so effective in the abundance ratio.

4. Discussion on the Anisotropy problem

In Figs. 1 and 2, we find two choices, a) $\alpha=1/3$ and b) $\alpha=1/2$, are both consistent with the experimental data, since the data nowadays available are too poor in the higher energy region, $\gtrsim 100\text{GeV}$ to decide which choice is better. It is well known, however, that the choice of $\alpha=1/2$ predicts too high amplitude of the anisotropy in comparison with those observed at TeV region, with as large as 0.1%[4], which is a severe constraint for the diffusion coefficient. So, we touch briefly upon the anisotropy based on our model, which is obtained by the gradient of the cosmic-ray density, $N_p(\mathbf{r})$.

Two components of the anisotropy amplitude in TeV region, δ_r along the Galactic plane and δ_z transverse to the disc, are easily given by

$$\delta_r \approx R^\alpha \frac{3D_0}{cr_Q}, \quad \delta_z \approx R^\alpha \frac{3D_0}{cz_Q} \frac{z_\odot}{z_D}, \quad \text{with } z_\odot \approx 10\text{pc}, \quad (7)$$

where we used two approximations, $r_Q \ll r_D$, $z_Q \ll z_D$, based on the analysis of the longitudinal and the latitudinal spreads of the diffused γ -ray[7].

Putting $D_0=10^{28}\text{cm}^2/\text{sec}$ at $R=1\text{GV}$, $r_Q=15\text{Kpc}$, $z_Q=0.15\text{Kpc}$, $z_D=1.2\text{Kpc}$, we find $\delta_r=6.8 \times 10^{-3}$, $\delta_z=2.8 \times 10^{-3}$ for $\alpha=1/2$ at 100TV, and $\delta_r=10^{-3}$, $\delta_z=4.2 \times 10^{-4}$ for $\alpha=1/3$ at 100TV. So the set, $(\gamma, \alpha)=(2.4 \sim 2.5, 1/3)$, is much preferable to another set, $(2.2 \sim 2.3, 1/2)$, from the constraint of the anisotropy amplitude. This point has been pointed out also by several authors[8].

Recently AGASA group reported a significant anisotropy of $\sim 4\%$ at 10^{18}eV [9], and it is interesting to note that Eq. (7) gives 3-4% at 10^{18}eV for $\alpha=1/3$ with use of the parameters expected from the present analysis. We had better, however, wait more reliable data on 2ry/1-ry ratio in TeV region to get a firm conclusion.

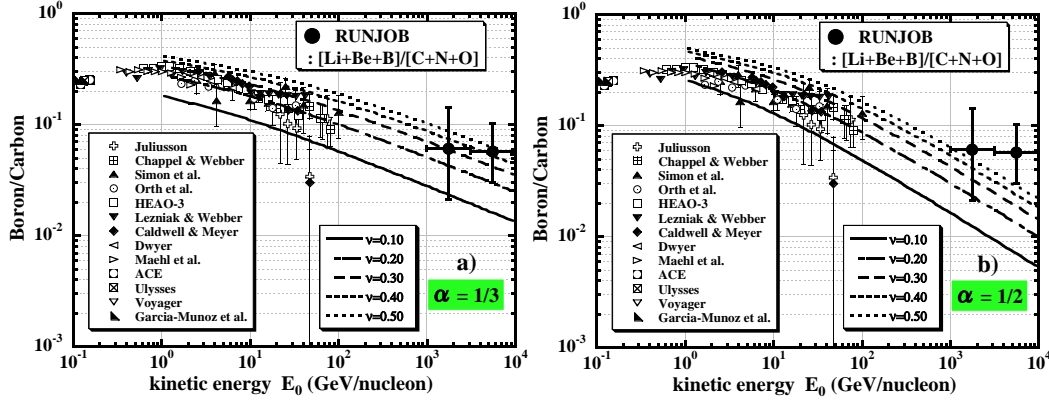


Fig. 1. Boron-carbon ratio with two curve-fittings, a) $\alpha = 1/3$ and b) $\alpha = 1/2$.

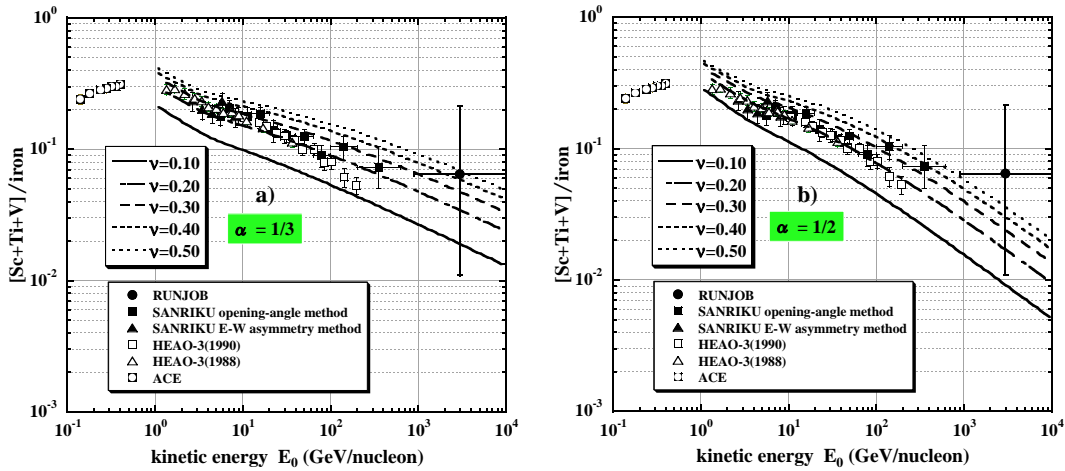


Fig. 2. subFe-iron ratio with two curve-fittings, a) $\alpha = 1/3$ and b) $\alpha = 1/2$.

1. Hareyama M., Nakazawa M., Saito C., Suzuki R., and Shibata T., in this proceeding (OG 1.3, ID 8516-1).
2. Shibata T., Hareyama M., Ito K., Nakazawa M., Saito C., and Suzuki R., in this proceeding (OG 1.3, ID 8455-2).
3. For instance, Heinbach U., and Simon M. 1995, ApJ 441, 209
4. Jones F.C., Lukasiak A., Ptsukin V., and Webber W. 2001, ApJ 547, 264
5. RUNJOB collaboration, in this proceeding (OG 1.1, ID 8715-2).
6. Webber W., Kish J., and Schrier D. 1990, Phys. Rev. C 41, 533
7. Shibata T., Hareyama M., Nakazawa M., Saito C., and Suzuki R., in this proceeding (OG 2.1, ID 8455-1).
8. Ptsukin V., Jones F.C, Lukasiak A., and Webber W. 2001, Proc. 27th ICRC 5, Hamburg, 1947
9. Teshima M. et al. 2001, Proc. 27th ICRC 1, Hamburg, 337